Composite chromium and graphene oxide as saturable absorber in ytterbium-doped *Q*-switched fiber lasers

Liming Liu, Haroldo T. Hattori,* Evgeny G. Mironov, and Abdul Khaleque

School of Engineering and Information Technology, UNSW Australia, Canberra ACT 2610, Australia

*Corresponding author: h.hattori@adfa.edu.au

Received 18 November 2013; revised 16 January 2014; accepted 21 January 2014;
posted 24 January 2014 (Doc. ID 201539); published 19 February 2014

In recent years, graphene and its compounds (e.g., oxides) have been used as saturable absorbers in passive *Q*-switched and mode-locked lasers, leading to the fabrication of compact pulsed fiber lasers. In this article, we study the operation of a *Q*-switched ytterbium-doped fiber ring laser based on a composite saturable absorber made of graphene oxide and chromium. We show that the addition of a thin layer of chromium can lead to pulse durations ranging from 3.5 to 9.4 μs and subsequently increasing the laser peak power.

OCIS codes: (140.3540) Lasers, Q-switched; (140.3615) Lasers, ytterbium; (140.3380) Laser materials.

http://dx.doi.org/10.1364/AO.53.001173

1. Introduction

Carbon is an essential component of life on Earth and has two stable (^{12}C and ^{13}C) and one radioactive (^{14}C) isotopes. Carbon has six electrons, which are distributed among $1s$, $2s$, and $2p$ orbital states. Electrons in carbon can form hybrid covalent bonds whereas one electron is distributed throughout the crystal, forming σ and π bonds [1]. In the case of graphene, atoms of carbon are arranged in a 2D honeycomb lattice with a nearest neighbor distance of about 1.42 Å. Graphene behaves like a zero-gap semiconductor [2], exhibiting many interesting properties, such as high electron mobility, strong nonlinear Kerr effects, high thermal conductivity, saturable absorption, and high mechanical strength [3,4]. The addition of hydroxyl, epoxyl, and carboxyl groups to the quasi-2D lattice of graphene leads to the creation of graphene oxide, which is easier to manipulate and attaches to many different materials without significant effort [5].

The optical properties of graphene arise from the interaction of photons and electrons in the structure: if the energy of the incoming photon is twice above its Fermi level, the linear absorption is about 2.3% per single graphene layer [1]; however, this absorption decreases at higher power levels, making graphene useful in saturable absorber and nonlinear optic applications. In addition to that, graphene-based devices can operate in a wide range of frequencies, from microwaves to optical frequencies, making graphene a good material for broadband applications.

Since the amount of light that is absorbed by graphene-based compounds changes with input power, graphene has been used as a saturable absorber in passive *Q*-switched and mode-locked lasers [4–12]. In contrast to semiconductor saturable absorbers (SESAMs), graphene can be easily deposited on the optical fiber end, does not require collimating devices such as lenses, and can operate over a wide range of wavelengths. In fact, graphene has already been used as a saturable absorber in

1559-128X/14/061173-08$15.00/0

many different doped fiber systems, such as erbium-doped [9] and thulium-doped [10,11] fiber lasers. In fact, the first thulium Q-switched/mode-locked graphene laser was reported by Ahmad *et al.* in 2012 [10].

Q-switching generally relies on initially preventing the laser cavity from oscillating while the population inversion is built in the active medium (the temporary halt of oscillations can be achieved by either removing the cavity feedback or strongly increasing the cavity losses) and thereafter restoring the cavity oscillations by drastically increasing its quality factor (Q) [13]: high peak optical pulses are then produced. The switching of the cavity Q can be achieved either actively (e.g., using an external modulator) or passively (e.g., using a saturable absorber). Some actively Q-switched lasers use acousto-optic modulators to deflect light from the cavity while the population in the upper level builds up [14–16] and then returns the optical beam back to the cavity by switching off the modulator. Another way to produce active Q-switching in optical fibers is by dynamically shifting the reflectivity peak of one of the grating reflectors by pumping the grating with a second pump laser [17]. Passive Q-switched lasers generally use saturable absorbers whose absorption depends upon the intensity of the incident light like graphene. In addition to graphene, other materials and fibers can be used as saturable absorbers such as thulium-doped fibers [18], Cr^{4+}:YAG and its compounds [19,20], semiconductor heterostructures [21], carbon nanotubes [12], and CaF_2 [22].

In addition to Q-switching, generation of high peak pulses can be produced by mode-locking [13] or gain-switching [23–25]. Mode-locked lasers generally produce shorter pulses than Q-switched and gain-switched lasers. In gain-switched lasers, the gain of the active medium is "externally controlled" by switching on/off the pump laser: when the pump laser is on, the laser reaches its threshold, and thereafter the population in the upper level builds up exponentially [23] and, when the pump is turned off, the population in the upper level decays rapidly producing short pulses. It generally does not require saturable absorbers and the scheme is especially attractive in the mid-infrared range where optical components are more expensive and harder to find. Moreover, gain-switched lasers are simpler, can operate in narrow linewidths and their principles can be extended to a wide variety of wavelengths [23].

Ultrafast lasers can be constructed by using either active or passive mode-locking [13]. Again, passive mode-locked lasers rely upon saturable absorbers, such as quantum well-based devices, carbon nanotubes, and graphene [12]. In contrast with quantum well-based saturable absorber, carbon nanotubes and graphene saturable absorbers do not require extensive alignment with the fiber, are cheaper, and can operate in a wide range of wavelengths with different doped fiber systems, such as Nd:YAG, erbium-, ytterbium-, and thulium-doped fibers. Peak powers as high as few hundred kilowatts and pulse durations as low as 60 fs have been achieved with carbon nanotube saturable absorbers, while sub-200 fs pulses have been achieved with graphene. Graphene can operate over a larger bandwidth than carbon nanotubes and quantum wells [12].

One of the main advantages of graphene oxide is that it can be purchased in powdered form and can be easily dissolved into water [9] or isopropryl alcohol [26]. Once the platelets are dispersed into a liquid solution, they can attach to the fiber end due to the thermophoresis effect [9], not requiring extensive chemical or material growth processes.

In addition to graphene oxide, other materials, such as chromium, have been used as saturable absorbers for ytterbium-doped fiber lasers. In this work, we study the effects of adding a thin layer of chromium to a graphene oxide saturable absorber. We show that the addition of an adequate thin layer of chromium can lead to a reduction in the pulse duration of Q-switched ytterbium-doped fiber laser.

2. Sample Preparation and Raman Spectrum

In order to produce graphene oxide, it is necessary to make graphite oxide first. Graphite oxide can be made by oxidizing graphite with different types of solutions such as a mixture of sulphuric acid and potassium permanganate (Hummers' method [27]). After making graphite oxide, graphene oxide can be produced by exfoliating graphite oxide. Both graphene and graphene oxide have been used in pulsed lasers [12], but graphene oxide is cheaper and more prone to mass production than graphene, can be easily bond to a large variety of polymers and materials, and is more chemically stable than graphene [28]. The electrical conductivity of graphene oxide is lower than graphene but the conductivity depends upon the degree of oxidation—in our case, we have less than 1% oxygen content according to the vendor [26], so the properties of the graphene oxide platelets should be very close to pure graphene. On the other hand, as argued by Paredes *et al.* [29], graphene oxide has more structural disorders than pristine graphene, which can lead to more scattering of light and larger losses.

In our case, we purchased graphene oxide powder from a commercial vendor [26]. The powder is then dispersed into isopropyl alcohol (IPA). After dispersing graphene oxide into IPA, the solution is mixed during 30 min by using an ultrasonic bath. Finally, the optical fiber is immersed in the graphene oxide solution, and some graphene platelets are attached to the fiber. Finally, the fiber is dried in a low power furnace during 20 min. As explained by Ahmad *et al.* [9], graphene oxide is then formed at the end of the fiber by thermophoresis [6]. After heating the fiber, IPA also completely evaporates, leaving only graphene platelets at the fiber end.

The Raman spectrum of the deposited graphene oxide layer is shown in Fig. 1. Three Raman modes can be identified in this spectrum: the G-mode, as a

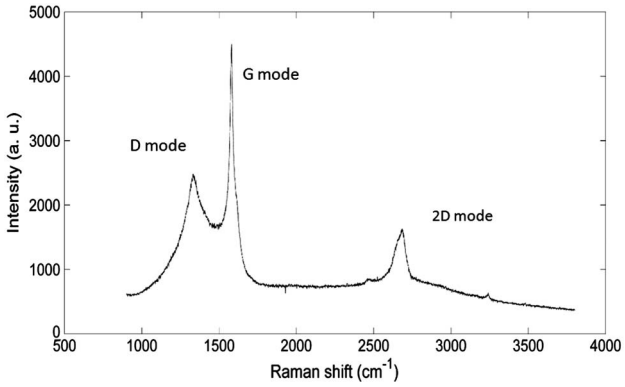

Fig. 1. Raman spectrum of the graphene oxide formed on the fiber's end.

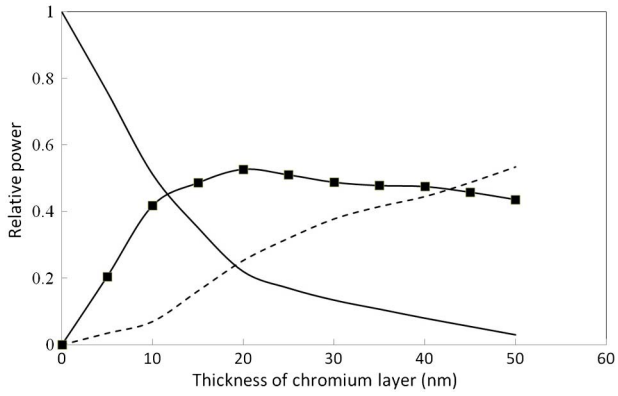

Fig. 2. Linear transmissivity (solid curve), reflectivity (dotted curve), and absorption (solid curve with square markers) for different thicknesses of chromium.

result of the bond stretching of sp^2 atoms in the crystalline structure; the D-mode, which arises from the breathing modes of sp^2 atoms in a ring, and the 2D-mode, which is the result of second-order two-phonon processes [5]. In a well-ordered graphene, the D-mode is very weak, and the 2D-mode is strong. The appearance of a strong peak for the D-mode indicates the presence of graphene oxide: the D-mode is related to disorder in the 2D lattice of graphene (in graphene oxide, there are out-of-plane bonds of carbon atoms with hydrogen and oxygen atoms [5]).

Whenever chromium is used, it is deposited on top of the graphene oxide layer by using an electron beam evaporator [30]. Metal thicknesses are varied from 10 to 100 nm. As an initial task, the low power absorption, reflectivity, and transmissivity of different thicknesses of chromium are calculated to understand the linear effects of adding chromium to the fiber, the calculations are based upon 3D FDTD simulations. The computational areas are terminated by perfectly matching layers and a Gaussian source with spot-size diameter of 6 μm is used in the simulations [31,32]. Light is launched into a fictitious optical fiber with refractive indices of 1.45 (core) and 1.44 (cladding), somewhat mimicking a typical weakly guiding optical fiber. A thin layer of chromium is sandwiched between two portions of fiber. Simulations are run at the free-space wavelength of 1094 nm where the emission of a ytterbium fiber laser is centered. Chromium is modeled as a lossy and dispersive medium with multiple resonant frequencies [33], and the dispersion data is imported from the material library of Fullwave software [34]. Figure 2 shows the transmissivity (solid curve), absorption (solid curve with square markers), and reflectivity (dotted curve) of a chromium layer as a function of its thickness. Based upon these simulations, it can be concluded that for thicknesses beyond 20 nm, chromium absorbs nearly 40%–50% of the incoming light. For thicknesses higher than 50 nm, chromium absorbs about 40%–50% of the incoming light while the remaining power is reflected; it should be emphasized that this is only true at low powers since at high powers, absorption of chromium reduces drastically.

3. Experimental Results

The experimental setup is shown in Figs. 3(a) (schematic of setup) and 3(b) (actual constructed fiber laser); it is, basically, a ring laser that is pumped by a 980 nm continuous wave (CW) laser coupled to a 100 μm multimode fiber. The power coupled to the multimode fiber can be varied from 0 to 1.5 W, but after passing through the WDM coupler, the maximum power is reduced to 800 mW. The CW laser can be externally modulated (ON–OFF shift keying) at a maximum repetition rate of 2 kHz (minimum repetition period of 0.5 ms). The duty cycle is chosen as 50%. The WDM coupler allows the 980 nm pump power to reach the double-cladding fiber, but does not allow any 1094 nm generated light to come back to the pump laser. After passing through the WDM coupler, 980 nm pump light travels through 6 m of double cladding highly doped ytterbium fiber (YB 1200-6/125 DC), in which the pump light propagates inside the first cladding while it is slowly absorbed by the core. The core diameter of YB 1200-6/125 DC is about 5.5 μm; thus the fiber is single-mode in the wavelength range around 1094 nm. After passing through 6 m of this ytterbium-doped fiber, more than 90% of the pump power is absorbed by the doped fiber core. When the ytterbium-doped fiber is pumped at

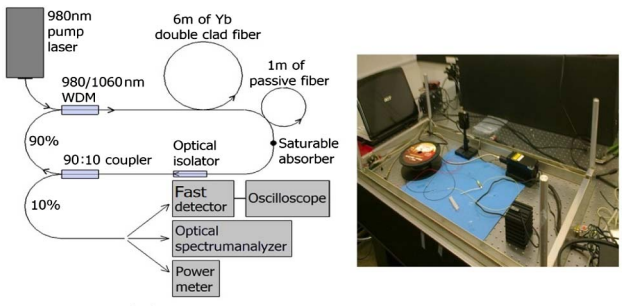

Fig. 3. (a) Schematic of the experimental setup using in our experiments. (b) Photograph of the constructed laser.

980 nm, it excites a laser transition from $^2F_{5/2}$ to $^2F_{7/2}$ energy levels of ytterbium atoms, resulting in an emission wavelength around 1094 nm. 1 m single-mode passive fiber (Corning HI 1060 fiber) is spliced to the YB-1200-6/125 DC fiber by using a FSM-70S commercial and professional fusion splicer; the passive fiber has a mode-field diameter of about 6 μm at 1060 nm (similar to the core diameter of the ytterbium-doped fiber), which keeps the single-mode signal at 1094 nm signal in the loop, but significantly dumps the remaining pumped power, which is not absorbed by the 6 m of ytterbium fiber (the measured pump power is reduced by more than 100 times after going through the passive fiber). At the other end of the fiber, the saturable absorber is placed and then connected to another single-mode fiber and an optical isolator. The optical isolator guarantees that the generated signal circulates only in the clockwise direction and avoids any spurious reflected signal to go back to the active ytterbium fiber. A 90:10 coupler is then used to couple 10% of the circulating laser signal to either a fast detector (rise time of 1 ns) followed by an oscilloscope, optical spectrum analyzer, or power meter. It should be mentioned that the circulating power is kept below 300 mW to avoid damaging the 90:10 coupler.

The absorption of photons (massless *Dirac Fermions*) in 2D periodic structures can be expressed in terms of the fine structure constant: the absorption coefficient $\alpha_{g,\mathrm{sl}}$ (percentage of the incident power that is absorbed by a single graphene layer) is given by [1]

$$\alpha_{g,\mathrm{sl}} = \frac{\pi c \mu_o e^2}{2h}, \tag{1}$$

where c is the speed of light in vacuum, μ_o is the magnetic permeability of vacuum, e is the elementary charge, and h is Planck's constant. Calculation of Eq. (1) shows that each graphene layer absorbs about 2.3% of the incident light when the energy of the incident photon is more than twice the Fermi energy level. Each graphene oxide platelet contains N_g layers of graphene, which are not uniformly spaced, meaning that the total absorption of each platelet is given by $N_g \alpha_{g,\mathrm{sl}}$; however, the number of platelets that are effectively attached to the fiber end is difficult to determine (the vendor informed that the average number of graphene layers per platelet is about six). Moreover, the aforementioned formula calculates the linear absorption while the overall absorption changes with the power that reaches the graphene oxide platelet. A more comprehensive formula for the absorption of a graphene platelet is given by [35]

$$\alpha_{\mathrm{go}} = \frac{\alpha_{\mathrm{nl}}}{1 + \frac{P_{\mathrm{circ}}}{I_{s,\mathrm{go}} A_{\mathrm{eff}}}} + \alpha_l, \tag{2}$$

where α_{go} is the absorption of the graphene platelet, α_{nl} is the nonlinear absorption coefficient as described in [16], P_{circ} is the power circulating the ring laser, A_{eff} is the effective area of the fiber, $I_{s,\mathrm{go}}$ is the saturation intensity of graphene (ranging from 0.61 to $0.71 \times 1010\ \mathrm{Wm^{-2}}$), and α_l is the linear absorption of graphene.

In principle, the total absorption of a combined chromium and graphene oxide saturable absorber can be modeled as

$$\alpha_{\mathrm{total}} = \alpha_{\mathrm{go}} + \mathrm{absa}_{\max}(1 - \alpha_{\mathrm{go}})\left[1 - \exp\left(\frac{-\alpha_{\mathrm{cr}} l_{\mathrm{cr}}}{1 + \frac{P_{\mathrm{circ}}}{I_{s,\mathrm{cr}} A_{\mathrm{eff}}}}\right)\right], \tag{3}$$

where α_{total} is the total absorption coefficient, α_{cr} is the linear absorption coefficient of chromium ($\sim 1.6 \times 108\ \mathrm{m^{-1}}$), $I_{s,\mathrm{cr}}$ is the saturation intensity of chromium with typical value of $1 \times 107\ \mathrm{Wm^{-2}}$), l_{cr} is the thickness of the chromium layer, and $\mathrm{absa}_{\max}$ is the maximum absorption for a given thickness. Note that chromium absorbs more light than graphene oxide and has significantly lower saturation intensity.

In the first experiment, the saturable absorber consists of only graphene oxide. The repetition rate is chosen as 1 kHz (our 980 nm CW laser is limited with repetition rates below 2 kHz). The peak pump power in Fig. 4(a) corresponds to 180 mW. The duration of the pulse (FWHM) is about 9.24 μs, which is similar to the duration of pulses in erbium (7.9 μs [9]) and thulium (10.5 μs [10]).

If the peak pump power is increased to 220 mW, multiple pulses start to appear in each period. This can be observed in Fig. 5(a) at a peak pump power $P_{\mathrm{pump}} = 250$ mW. The duration of the main pulse also decreases as power increases. Figure 5(b) shows the emission spectrum, whose shape is similar to the one found in [9]. The emission peak is broad with several peaks as was observed by Ahmad *et al.* [9]. Because of our detector limitation, it is difficult to observe the whole peak; however, as can be seen in Fig. 5(b), the lasing peak is centered around 1095 nm. The spectrum in Fig. 5(b) seems to be cut at wavelengths above 1100 nm because the photodetector of the spectrum analyzer is made of silicon: silicon detectors have a cut-off wavelength close to 1100 nm. In addition to that, the spectrum in Fig. 5(b) exhibits multiple peaks because of

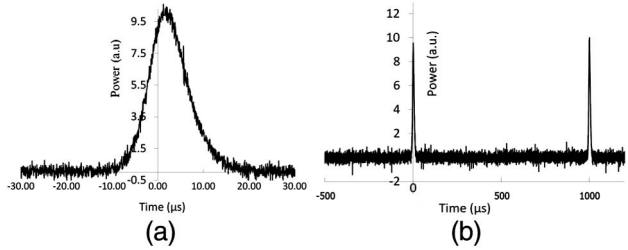

Fig. 4. (a) Pulse generated by graphene oxide Q-switched ytterbium laser. (b) Sequence of pulses at a repetition rate of 1 kHz.

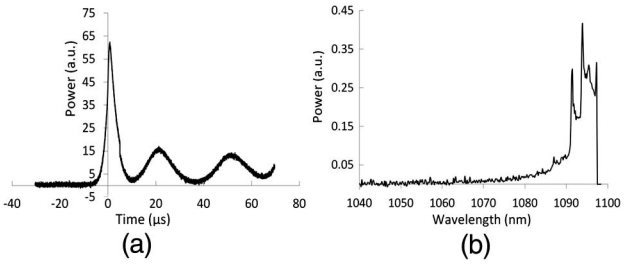

Fig. 5. (a) Sequence of pulses at $P_{\text{pump}} = 250$ mW. (b) Power spectra of the Q-switched laser with graphene oxide only.

perturbations in the cavity and the presence of multiple longitudinal modes in the gain spectrum of the laser [9].

In case that, only chromium is used as saturable absorber, the variation of chromium thickness (from 5 to 40 nm) in the ring resonator does not significantly change the pulse duration. The average pulse duration of the Q-switched pulses remains roughly 4.5 μs. If the pump power is increased, secondary pulses start to appear in each period similarly to what is shown in Fig. 5(a).

When a thin layer of chromium is added to graphene oxide, the duration of Q-switched pulses changes with chromium thickness as shown in Fig. 6: the duration of the pulses is initially 9.4 μs (graphene oxide only), decreases as the chromium layer becomes thicker and then reaches saturation at thicknesses above 50 nm (large amount of chromium masks the presence of graphene oxide). It is interesting to note that the duration of the pulses reaches a minimum when the thickness of chromium is about 30 nm; the minimum duration of the pulse is about 3.5 μs somewhat below the average duration of pulses with only a thin layer of chromium. The laser was left to operate over 30 min for each thickness, and the pulse profile remained the same. The square markers show the experimental data points in the plot while the solid curve is an average interpolated curve of the experimental data.

The presence of chromium affects the saturable absorber in different ways, such as shifting the Fermi level of the graphene layers [35] and increasing the

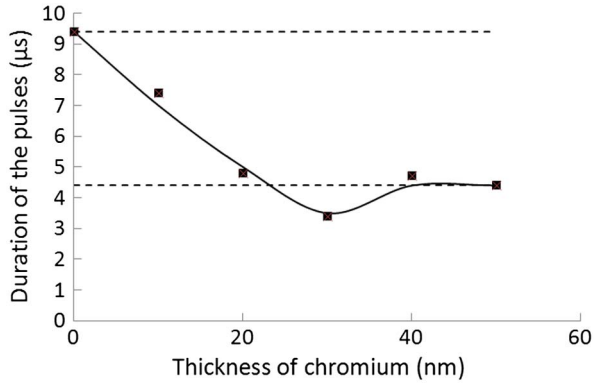

Fig. 6. Duration of pulses as a function of the thickness of chromium layer.

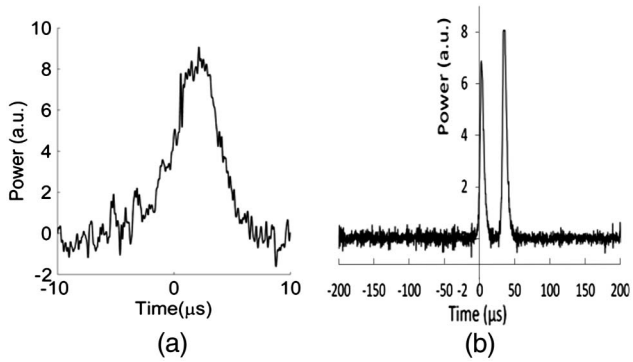

Fig. 7. (a) Single pulse at peak pump = 200 mW. (b) Two pulses at peak pump = 300 mW.

absorption of light in the saturable absorber; the overall absorption of light is increased and the saturation intensity is reduced as well. In fact, in Q-switched lasers, it is desirable to have a high nonsaturable absorption and low-saturation intensity; [36] what is achieved by the addition of chromium.

Figures 7(a) and 7(b) show pulses for 30 nm of chromium added to graphene oxide at different power levels: (a) at $P_{\text{pump}} = 200$ mW when a single pulse per repetition period is observed and (b) at $P_{\text{pump}} = 300$ mW when two pulses per repetition period are observed. At $P_{\text{pump}} = 200$ mW, the duration of the pulse is about 3.5 μs. We observed a single pulse from the peak pump threshold level to about $P_{\text{pump}} = 250$ mW.

We measured the reflectivity (R_{lp}) and transmissivity (T_{lp}) at low power for different thicknesses of chromium (l_{cr}) and the results are shown in Table 1.

From Table 1, it can be observed that the highest absorption takes place for a chromium thickness of 30 nm, giving an initial indication that we may expect a higher modulation depth for this thickness. The spot size diameter in the measurements was 10 μm, but the power that actually reached the sample through the micro-photoluminescent setup was considerably lower than the incident power.

We plot the total absorption [Eq. (3)] as a function of the circulating power (P_{circ}) in Fig. 8. The values of absorption for chromium at low powers are taken from our measured values while other parameters for chromium and graphene oxide are taken from Bao *et al.* [35] and Oliveira and Zilio [37]. In this plot, it is assumed that the spot size diameter is 6 μm to simulate our fiber. The solid curve shows absorption

Table 1. Measured Reflectivity (R_{lp}) and Transmissivity (T_{lp}) as a Function of the Chromium Thickness (l_{cr}) for Low Incident Power ($P = 5$ mW); Absorption is Calculated as $A_{\text{lp}} = 1 - R_{\text{lp}} - T_{\text{lp}}$

l_{cr} (nm)	T_{lp}	R_{lp}	A_{lp}
20	0.21	0.32	0.47
30	0.15	0.35	0.50
40	0.09	0.43	0.48

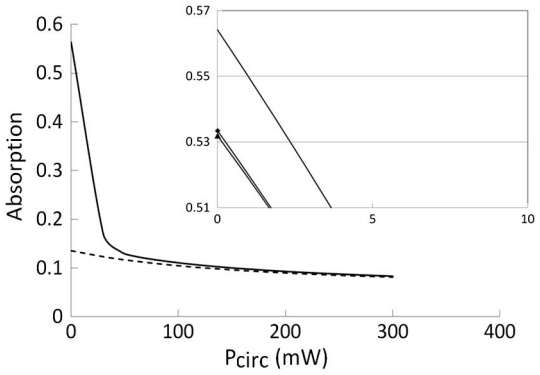

Fig. 8. Absorption of graphene oxide (dotted curve), graphene oxide, and 30 nm of chromium and graphene oxide as a function of the circulating power. The inset shows the absorption for low powers for 20 nm of chromium (solid curve with triangular marker), 30 nm (solid curve) and 40 nm (solid curve with rhombic marker) plus graphene oxide.

as a function of P_{circ} for 30 nm of chromium plus graphene oxide (solid curve) and solely graphene oxide (dotted curve). It is evident that, at low powers, the addition of chromium leads to a significantly increase of the absorption of the saturable absorber and that chromium saturates much faster than graphene oxide. The two curves converge at high powers, but the modulation depth increases considerably with the addition of chromium. In the inset of Fig. 8, it can be observed that the highest nonsaturable absorption occurs for a thickness of 30 nm (solid curve), leading to a higher nonsaturable absorption and a higher modulation depth; a higher modulation depth $l_{\text{cr}} = 30$ nm would lead to shorter pulses. For thicker layers of chromium, not only the absorption of chromium increases but so its reflectivity.

Figure 9 shows the average circulating power (P_{circ}) as a function of the peak pump power (P_{pump}). As mentioned before, the duty cycle of the pump pulses is 50% with a repetition rate of 1 kHz. The data with square and triangular markers correspond to the cases when only graphene oxide and graphene oxide plus 30 nm of chromium are used, respectively. The higher absorption of chromium leads to lower circulating power as is observed in Fig. 9, but not significantly lower since only a small amount of chromium is being used.

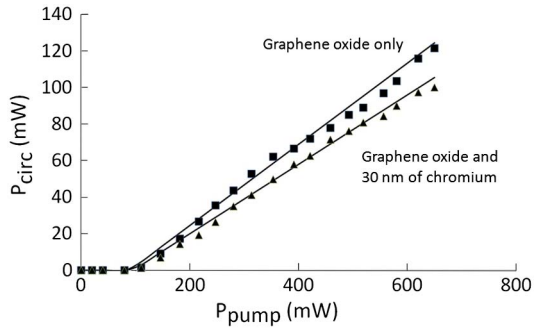

Fig. 9. Average circulating power (P_{circ}) as a function of the peak pump power (P_{pump}).

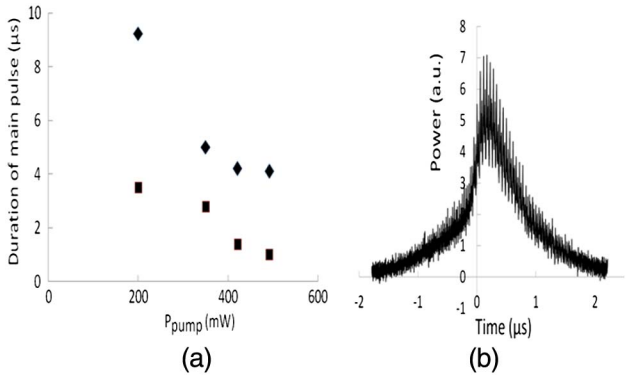

Fig. 10. (a) Duration of the main pulse as a function of peak pump power (P_{pump}). (b) Main peak at $P_{\text{pump}} = 400$ mW.

The duration of the main pulse changes with peak pump power (P_{pump}) as shown in Fig. 10(a). When only graphene oxide is used [rhombic markers in Fig. 10(a)], the duration of the main pulse decays almost exponentially with the increase of peak pump power, until it reaches saturation at higher powers. The behavior is different when 30 nm of chromium is added to graphene oxide; the rate of change in duration is slower as can be seen in the data points with square markers, and the pulse duration reaches values below 800 ns [as shown in the inset in Fig. 10(b)]. However, it should be reminded that, at high pump powers, multiple peaks appear in the repetition period. These peaks could be merged together if the repetition rate is increased, as was done in [9], but might become a problem at low repetition rates and is a result of relaxation of carriers in the gain medium. Also the separation between neighboring pulses change with the pump power what is undesirable.

The presence of "spikes" in the pulse shown in Fig. 10(b) seems to indicate a transition to an intermediate state, which is called Q-switching mode-locked regime [21]: an increase of power can lead to significantly shorter pulses in the repetition period. The average circulating power can be calculated as

$$P_{\text{circ}} = \frac{1}{T_r}\int_{-0.5T_r}^{0.5T_r} P_{\text{env}}(t)\mathrm{d}t, \tag{4}$$

where $P_{\text{env}}(t)$ is the envelope function of the circulating power and T_r is the repetition period. The peak power can be roughly estimated as

$$P_{\text{peak}} \approx P_{\text{circ}} T_r / t_{\text{mainpeak}}, \tag{5}$$

where t_{mainpeak} is the FWHM duration of the main peak. For example, at $P_{\text{pump}} = 200$ mW, the duration of the pulses are 8.4 and 3.4 μs for graphene oxide only and composite mixture of graphene oxide and 30 nm of chromium, respectively, leading to peak pulses of approximately 2.70 and 4.85 W, respectively.

4. Conclusions

In this article, we studied a composite saturable absorber made of a mixture of chromium and graphene oxide. The addition of 30 nm of chromium leads to a reduction in the duration of pulses to 3.5 μs, which could be attributed to a larger nonsaturable absorption of light by chromium and its reduced saturation intensity. The properties of chromium become predominant over graphene oxide when the thickness of chromium exceeds 40 nm. The peak power can also be increased by the addition of a thin layer of chromium. The laser operated steadily with the addition of a thin layer of chromium at high powers, and the duration of pulses could reach 800 ns but at the expense of generating additional secondary pulses.

The authors gratefully acknowledge the financial support from the Australian Research Council (ARC) and UNSW Australia. We would also acknowledge the technical support provided by Mr. Darryl Budarick (UNSW Australia) in training students to handle optical fibers and Mr. Antonio Galvao for his suggestions. Mr. Wen Jun Toe and Dr. Peter Reece (UNSW Australia) are gratefully acknowledged for conducting the absorption experiments in this paper. We finally thank Dr. Dragomir Neshev (The Australian National University) for useful discussions on the results.

References

1. M. I. Katsnelson, *Graphene: Carbon in Two Dimensions* (Cambridge University, 2012).
2. I. M. Tsidikovskii, *Band Structures of Semiconductors* (Oxford, 1982).
3. F. Bonaccorso, Z. Sun, T. Hasan, and A. C. Ferrari, "Graphene photonics and optoelectronics," Nat. Photonics **4**, 611–622 (2010).
4. A. Martinez and Z. Sun, "Nanotubes and graphene saturable absorbers for fibre lasers," Nat. Photonics **7**, 842–845 (2013).
5. J. H. Warner, F. Schäffel, A. Bachmatiuk, and M. H. Rümmeli, *Graphene: Fundamentals and Emergent Applications* (Elsevier, 2013).
6. A. Martinez, K. Fuse, B. Xu, and S. Yamashita, "Optical deposition of graphene and carbon nanotubes in a fiber ferrule for passive mode-locked lasing," Opt. Express **18**, 23054–23061 (2010).
7. Y. Yap, R. M. De La Rue, C. Pua, S. Harun, and H. Ahmad, "Graphene-based *Q*-switched pulsed fiber laser in a linear configuration," Chin. Opt. Lett. **10**, 041405 (2012).
8. T. Hasan, Z. Sun, F. Wang, F. Bonaccorso, P. H. Tan, A. G. Rozhin, and A. C. Ferrari, "Nanotube-polymer composites for ultrafast photonics," Adv. Mater. **21**, 3874–3899 (2009).
9. H. Ahmad, F. D. Muhammad, M. Z. Zulkifli, and S. W. Harun, "Graphene oxide based saturable absorber for all-fiber *Q*-switching with a simple optical deposition technique," IEEE Photon. J. **4**, 2205–2213 (2012).
10. H. Ahmad, A. Z. Zulkifli, K. Thambiratnam, and S. W. Harun, "2.0 μm *Q*-switched thulium-doped fiber with graphene oxide saturable absorber," IEEE Photon. J. **5**, 1501108 (2013).
11. B. Lu, H. Chen, M. Jiang, X. Chen, Z. Ren, and J. Bai, "Graphene-based passive *Q*-switching for a 2 μm thulium doped fiber laser," Laser Phys. **23**, 045111 (2013).
12. Z. Sun, T. Hasan, and A. C. Ferrari, "Ultrafast lasers mode-locked by nanotubes and graphene," Physica E **44**, 1082–1091 (2012).
13. A. E. Siegman, *Lasers* (Stanford University Science Books, 1986).
14. H. Zhao, Q. Lou, J. Zhou, F. Zhang, J. Dong, Y. Wei, L. Li, and Z. Wang, "An acousto-optic *Q*-switched fiber laser using China-made double-cladding fiber," Chin. Opt. Lett. **5**, 522–523 (2007).
15. Y. Chen, Y. Lin, X. Gong, B. Huang, Z. Luo, and Y. Huang, "Acousto-optic *Q*-switched self-frequency-doubling Er:Yb: $YAl_3(BO_3)_4$ laser at 800 nm," Opt. Lett. **37**, 1555–1567 (2012).
16. M. Delgado-Pinar, D. Zalvidea, A. Díez, P. Péres-Millán, and M. V. Andrés, "*Q*-switching of an all-fiber laser by acousto-optic modulation of a fiber Bragg grating," Opt. Express **14**, 1106–1112 (2006).
17. R. J. Williams, N. Jovanovic, G. D. Marshall, and M. J. Withford, "All-optical, actively *Q*-switched fiber laser," Opt. Express **18**, 7714–7723 (2010).
18. T. Y. Tsai, Y. C. Fang, and S. H. Huang, "Passively *Q*-switched erbium all-fiber lasers by use of thulium-doped saturable-absorber fibers," Opt. Express **18**, 10049–10054 (2010).
19. X. Zhang, A. Brenier, J. Wang, and H. Zhang, "Absorption cross-sections of Cr^{4+}:YAG at 946 nm and 914 nm," Opt. Mater. **26**, 293–296 (2004).
20. S. Forget, F. Druon, F. Balembois, P. Georges, N. Landru, J. P. Feve, J. Lin, and Z. Weng, "Passively *Q*-switched diode-pumped Cr^{4+}:YAG/Nd^{3+}:$GdVO_4$ monolithic microchip laser," Opt. Commun. **259**, 816–819 (2006).
21. U. Keller, K. J. Weingarten, F. X. Kärtner, D. Kopf, B. Braun, I. D. Jung, R. Fluck, C. Hönninger, N. Matuschek, and J. A. der Au, "Semiconductor saturable absorber mirrors (SESAM's) for femtosecond to nanosecond pulse generation in solid-state lasers," IEEE J. Sel. Top. Quantum Electron. **2**, 435–453 (1996).
22. L. Su, D. Zhang, H. Li, J. Du, Y. Xu, X. Liang, G. Zhan, and J. Xu, "Passively *Q*-swicthed Yb^{3+} laser with Yb^{3+}-doped CaF_2 crystal as saturable absorber," Opt. Express **15**, 2375–2379 (2007).
23. J. Yang, Y. Tang, and J. Xu, "Development and applications of gain-switched fiber lasers," Photon. Res. **1**, 52–57 (2013).
24. S. Jackson and T. A. King, "Efficient gain-switched operation of a Tm-doped silica fiber laser," IEEE J. Quantum Electron. **34**, 779–789 (1998).
25. A. M. Heidi, Z. Li, P. C. Shardlow, M. Becker, M. Rothhardt, M. Ibsen, R. Phelan, B. Kelly, S. U. Alam, and D. J. Richardson, "100 kW peak power picosecond thulium-doped amplifier system seeded by a gain-switched diode laser at 2 μm," Opt. Lett. **38**, 1615–1617 (2013).
26. http://www.kemix.com.
27. W. S. Hummers and R. E. Offeman, "Preparation of graphitic oxide," J. Am. Chem. Soc. **80**, 1339 (1958).
28. D. Wang, X. Zhang, J. W. Zha, J. Zhao, Z. M. Dang, and G. H. Hu, "Dielectric properties of reduced graphene oxide/polypropylene composites with ultralow percolation threshold," Polymer **54**, 1916–1922 (2013).
29. J. I. Paredes, S. Villar-Rodil, P. Solis-Fernández, A. Martínez-Alonso, and J. M. D. Tascón, "Atomic force and scanning tunneling microscopy imaging of graphene nanosheets derived from graphene oxid," Langmuir **25**, 5957–5968 (2009).
30. Z. Li, H. T. Hattori, P. Parkinson, J. Tian, L. Fu, H. H. Tan, and C. Jagadish, "A plasmonic staircase nano-antenna device with strong electric field enhancement for surface enhanced Raman scattering (SERS) applications," J. Phys. D **45**, 305102 (2012).
31. H. T. Hattori, "Analysis of optically pumped equilateral triangular microlasers with three mode-selective trenches," Appl. Opt. **47**, 2178–2185 (2008).
32. R. M. Cazo, C. L. Barbosa, H. T. Hattori, and V. M. Schneider, "Steady-state analysis of a directional square lattice

band-edge photonic crystal lasers," Microw. Opt. Technol. Lett. **46**, 210–214 (2005).
33. H. T. Hattori, Z. Li, D. Liu, I. D. Rukhlenko, and M. Premaratne, "Coupling of light from microdisk lasers and plasmonic nano-antennas," Opt. Express **17**, 20878–20884 (2009).
34. Fullwave 6.1 RSOFT Design Group, 2008 [Online] Available: http://optics.synopys.com.
35. Q. Bao, H. Zhang, Y. Wang, Z. Ni, Y. Yan, Z. X. Shen, K. P. Loh, and D. Y. Tang, "Atomic-layer graphene as a saturable absorber for ultrafast pulsed lasers," Adv. Funct. Mater. **19**, 3077–3083 (2009).
36. M. Bokdam, P. A. Khomyakov, G. Brocks, and P. J. Kelly, "Field effect doping of graphene in metal/dielectric/graphene heterostructures: a model based upon first-principles calculations," Phys. Rev. B **87**, 075414 (2013).
37. L. C. Oliveira and S. C. Zilio, "Chromium-doped saturable absorbers investigated by the Z-scan technique," Braz. J. Phys. **24**, 498–501 (1994).